Matrix Biology 2023; 120: 60-75 (DOI: 10.1016/j.matbio.2023.05.005)

HS3ST3 activity on CD138 increases multiple myeloma aggressiveness

Baert L.[1]†#, Manfroi B.[1]‡#, Quintero M.[2], Chavarria 0.[1]§, Barbon P.V.[1]||, Clement E.[2], Zeller A.[3]¶, Van Kuppevelt T.[4], Sturm N.[2,5], Moreaux J.[6,7], Tveita A.[8], Bogen B.[8,9], McKee T.[10] and B. Huard[2*]

[1]Institute for Advanced Biosciences, University Grenoble-Alpes, INSERM U1209, La Tronche, France.
[2]translational innovation in medicine and complexity, University Grenoble-Alpes, CNRS UMR5525, La Tronche, France.
[3]Department of Pathology and Immunology, university Hospitals, Geneva, Switzerland.
[4]Rabdoud university medical center, Nijmegen, the Netherlands
[5]Department of Pathology, university Hospital, Grenoble, France.
[6]Department of Biological Hematology, University Hospital, Montpellier, France.
[7]Institute of Human Genetics, centre national de la recherche scientifique, University Montpellier, France.
[8]Department of Immunology and transfusion medicine, Institute for Immunology, university Hospital, Oslo, Norway.
[9] University of Oslo, Norway.
[10] Department of clinical pathology, university Hospitals, Geneva, Switzerland.
Present addresses:
† Division of Rheumatology and Immunology, Department of Internal Medicine, College of Medicine, Columbus, Ohio, USA ‡Institute Necker Enfants malades, institut national de la santé et de la recherche médicale U1151, Paris, France, §Department of Genomics and Proteomics, Gorgas Memorial Institute, Panama, Republic of Panama, ||Center of Immunology, Marseille-Luminy, Marseille, France. ¶Covance central laboratory services SA, Meyrin, Switzerland,

# These authors contribute equally to this work

Corresponding author:
Bertrand Huard
Jean-Roget building, domaine de la merci, 38700 La Tronche, France
Bertrand.huard@univ-grenoble-alpes.fr
+33457421891

Authors declare no conflict of interest

Abstract:

Multiple myeloma is a hematological neoplasm derived from plasma cells invariably developing in the bone marrow (BM). The persisting clinical challenge in MM resides in its high ability to resist drugs as shown by the frequent relapses observed in patients regardless of the treatment applied. In a mouse model of MM, we identified a subpopulation of cells harboring increased resistance to current MM drugs. These cells bound a proliferation inducing ligand (APRIL), a key MM promoting/survival factor. APRIL binding involved the heparan sulfate (HS) chain present on CD138, and correlated with reactivity to the anti-HS antibody 10e4. $10e4^+$ cells had a high proliferation activity, and were able to form colonies in 3-D cultures. $10e4^+$ cells were the only cells able to develop in BM after intravenous injection. They also resisted drugs *in vivo*, since their number increased after treatment in BM. Notably, $10e4^+$ cells differentiated into $10e4^-$ cells upon *in vitro* and *in vivo* expansion. Expression of one sulfotransferases, HS3ST3a1, allowed modification of CD138 to confer reactivity to 10e4 and binding to APRIL. *HS3ST3a1* deletion inhibited tumorigenesis in BM. Notably, $10e4^+$ and $10e4^-$ populations coexisted at a variable frequency in the BM of MM patients at diagnosis. In total, our results identify a post-translational modification on the extracellular part of CD138 defining aggressive MM cells, which may be targeted to better control drug resistance.

Keywords: multiple myeloma, CD138, heparan sulfate proteoglycan, APRIL, drug resistance

Introduction

Multiple myeloma (MM) is the most common form of hematologic tumors derived from plasma cells. MM patients are benefiting from highly efficient drugs including immunomodulatory agents, and proteasome inhibitors [1]. Nevertheless, frequent relapses are still observed, highlighting a high ability to resist drugs for this tumor. MM invariably develops in the bone marrow (BM), showing the strong dependency of this tumor on its microenvironment. One sensor of the MM microenvironment is the CD138 molecule. CD138 acts as a key receptor for MM, since its RNA interference strongly impairs MM development [2]. The latter is explained by the fact that CD138 acts as a coreceptor for several MM survival/promoting factors [3]. Among these factors are one member from the TNF superfamily, a proliferation inducing ligand (APRIL, TNFSF13), the hepatocyte growth factor (HGF) and Wnts [4][5][6]. CD138 also participates to tumor-induced neoangiogenesis by binding to the vascular endothelial growth factor (VEGF) [7]. CD138 is a glycosaminoglycan (GAG) belonging to the syndecan family, also called syndecan-1 [8]. It is the only GAG expressed by MM cells [9][10]. Its function heavily relies on its GAG moiety [11]. As relevant examples, MM pre-treatment with heparitinase, a bacterial enzyme able to digest the GAG chain, and knock-down by RNA interference of EXT-1, an enzyme involved in the elongation of the GAG chain inhibits *in vivo* MM development [12]. GAGs are glycosidic chains composed of a repetitive disaccharide motif. Depending on the dissacharide unit, GAGs are classified either as heparan sulfate (HS) or chondroitin sulfate (CS) chains. CD138 has a mix composition of HS and CS chains with three potential canonical serine-glycine sequences for GAG attachment at its membrane-distal N-terminus and one at its membrane-proximal domain [13]. The three N-terminus sites for HS anchor cooperates to promote MM [14]. The sulfation pattern on HS and CS chains varies depending on the activities of sulfotransferases, which modulates ligand binding [15]. Here,

we are showing that activity of a single HS sulfotransferase (HSST) strongly modulates MM behavior.

Material and methods

Mouse and human experimentation

Mouse experimentation followed the ARRIVE guidelines and was approved by a relevant veterinary office. Balb/c mice were obtained from Charles River. MOPC-315 cells were injected intravenously in 0.1 ml PBS via the tail vein. At the first sign of hind limb paralysis corresponding to compression of the spine, mice were euthanized. The experiments using human materials were approved by a relevant ethic committee, and conducted according to the declaration of Helsinki. Samples were obtained after patients' informed consent.

Cells

The human MM cell line L363 was obtained from the American tissue culture collection. The parental MOPC-315 cell line and its variant have been described elsewhere [16]. Cells were cultured in RPMI-1640 with glutamax (Gibco), 10% heat inactivated fetal bovine serum (Eurobio) and 1 mM sodium pyruvate (Gibco). Cells were seeded at 0,3 cells per well in round bottom 96 well plates for cloning by limiting dilution. The clonogenic growth was measured by plating 1 x 10^5 cells in 12-well plates containing RPMI-1640 medium with 1.27% methylcellulose (Merck) and 10% fetal bovine serum. Plates were incubated 3 weeks at 37°C. Colonies with more than 10 cells were counted.

Gene inactivation by CRISPR/Cas9

Generation of *HS3ST3a1*-deficient tumor cells was performed according to a previously published protocol with RNA guide sequences designed using the online service CHOPCHOP[17],[18]. The following guide sequences were utilized: HS3ST3a1#1: 5'- GAGGGGGCCATCCTAGC-3', HS3ST3a1#2: 5'- GACCCAGGGAACTGGCGATG-3'. Cells were electroporated using an Amaxa Nucleofector II (Lonza), and GFP-positive cells were single-cell sorted using a FACSAria II (BD Biosciences).

mRNA expression analysis

Total RNA was extracted with the RNeasy micro kit (Qiagen) and cDNA generated using oligo(dT)$_{12\text{-}18}$ and the SuperScript II reverse transcriptase (Thermo Fisher). Primers used in qRT-PCR are described in table 1sup. Quantification was performed using the iCycler iQ Real-Time PCR Detection system (Bio-Rad) and a SYBRgreen-based kit (iQ SupermixBio-Rad). Expression levels were normalized using mouse actin mRNA. Results were quantified using a standard curve generated with serial dilutions of input DNA.

Recombinant protein

Flag-tagged mouse APRIL$_{A88}$ (88-232) and its control mouse CD40-L (115-260) were purchased from Adipogen. Amplicons for mouse VEGF and HGF were synthetized from RNA of mouse BM with Taq platinum polymerase (Invitrogen). The soluble coding sequence of mouse VEGF-A was cloned with the forward primer (5'-GCGTCGACGCACCCACGACAGAAGGAG-3') and the reverse primer (5'-GCGAATTCTCACCGCCTTGGCTTGTC-3'). For mouse HGF (5'-GCGTCGACCAGAAGAAAAGAAGAAATAC-3') and (5'-

GCGGATCCCTACCGCAGTTGTTTTGTTTTGC-3') were used. Amplified products were cloned into a modified pCR-III plasmid encoding for the FLAG peptide at the N-terminus of the recombinant proteins. DNA sequencing was performed with the T7 and Sp6 primers at Eurofins. Corresponding recombinant soluble mouse VEGF (aa 27 to 214) and HGF (aa 32 to 495) were produced by transient transfection with polyethylenimine (PEI) of HEK-293T cells (American tissue culture collection). Supernatants produced in serum-free Opti-MEM culture medium (Gibco), and collected 6 days post transfection were analyzed by Western-blot after protein separation on a SDS-PAGE and transferred to a PVDF membrane (Bio-Rad). The membrane was blocked with PBS, Tween 20 0.3%, BSA 5%, and stained with biotinylated anti-FLAG (clone M2, Sigma), followed by streptavidin HRP (Sigma) and clarity western ECL substrate (Bio-Rad). Chemiluminescence was acquired with a ChemiDoc^{TM} (Bio-Rad). Supernatants were concentrated 10X by centrifugation on an amicon filter (Merck-Millipore) with a size exclusion of 3 kDa before being used in staining procedures.

Flow cytometry

The anti-HSPG mAb 10e4 (mouse IgM) and 3g10 (mouse IgG2b) were obtained from Amsbio, and their binding was revealed with a goat anti-mouse IgM and IgG, respectively, conjugated to FITC (BD Biosciences). HS4C3 binding was detected with a polyclonal antibody against the VSV tag (Abcam). Biotinylated-anti-mouse BCMA (Vicky-2, rat IgG) and TACI (1A10, rat IgG) were obtained from Enzo life sciences, and their binding was revealed with phycoerythrin (PE)-conjugated streptavidin (BD Biosciences). PE-conjugated anti-mouse CD138 (clone 281-2, rat IgG) and Ki67 (clone B56, mouse IgG) were from BD biosciences. Binding of flag-tagged recombinant proteins was revealed with biotinylated anti-FLAG (clone M2, mouse IgG, Sigma)

followed by PE-streptavidin. All antibodies were used at 10 µg/ml. Inhibitions of APRIL binding with heparin, NaClO3, heparitinase and chondroitinase were performed as previously described [19–21]. Surface staining on viable cells was performed according to standard procedures. Dead cells were excluded by 7-AAD (BD Biosciences) staining. For cell clump analysis, cell centrifugation was replaced by a 5-mn period of cell sedimentation, and fluorescence was acquired at the lowest fluidic rate. Total stainings were performed after fixation of cells with 1% formaldehyde and permeabilization with 1% saponin. Excess formaldehyde was quenched with 50 mM NaCl. Fluorescence was analyzed on a Accuri C6, and FACS-sorting was performed on a FACS-ARIA, both from BD Biosciences. MACS-sorting was performed on MS columns according to manufacturer's instructions with 10e4 and anti-mouse IgM magnetic beads (Myltenyi Biotec). Two cycles were applied for the negative population. Purity was assessed by cytofluorimetry by restaining with 10e4 and fluorochrome-conjugated anti-mouse IgM.

Immunohistochemistry and cytology

Immunochemistry was performed according to standard procedures. 10e4 and the anti-human CD138 (clone MI15, mouse IgG, Dako) staining required no and a citrate-based heat-induced epitope retrieval, respectively. The multiplex staining was performed as previously described [22]. 10e4 staining was followed by anti-CD138. Staining. Stained sections were scanned with Scanscope Aperio (Leica) at a magnification of 40X. Antibody removal was confirmed by restarting the staining procedure at the secondary antibody stage. Images from scanned files were treated with Calopix (Tribvn healthcare). Cytospins from FACS-sorted cells were examined by Papanicolaou staining. Microscopy images were visualized with a AxioImager M2 microscope (Zeiss). Cell cultures were imaged with an inverted AxioObserver Z1 microscope (Zeiss).

Serum calcium measurement

Serum calcium concentration was measured on whole mouse blood with the calcium colorimetric assay kit according to manufacturer's instructions (Biovision).

Drug treatment

Lenalidomide, dexamethasone, bortezomib and melphalan were obtained from Sigma. MOPC-315 cells were plated in triplicates at 1 x $10e^4$ cells per well of flat bottom 96 well plates and treated for 48 hours with drugs. Cell viability was assessed with 3-(4,5-dimethylthiazol-2-yl)-2,5-diphenyltetrazolium bromide-based chromogenic assay. For *in vivo* experiments, melphalan was injected intraperitoneally at 5 mg/kg on day 20, 23 and 27 after tumor cell intravenous injection. 10e4 reactivity was assessed by flow cytometry on day 28 on flushed BM cells.

Statistics

Means +/- standard deviations are shown. Statistical analysis was performed using GraphPad Prism software. Normality of data set distribution was tested with the D'Agostino and Pearson or Shapiro Wilk for low size data sets. Accordingly, parametric and non-parametric two-tailed *t*-tests were performed. Significant differences were defined as $p < 0.05$.

Results

A fraction of MOPC-315$_{BM}$ cells binds APRIL and 10e4

The MOPC-315$_{BM}$ variant cell line was derived from the MOPC-315$_{WT}$ parental cell line by its unique ability to develop in the BM of syngeneic Balb/c mice after intravenous injection [16]. Both cell lines develop equally well in the spleen, and can be propagated *in vitro*. We first observed

that a fraction of cells among the MOPC-315$_{BM}$ variant cell line bound APRIL, despite the fact that all cells expressed similar levels of the two APRIL signaling receptors, a transmembrane activator and CAML interactor (TACI) and the B-cell maturation antigen (BCMA), as well as the APRIL-coreceptor on MM cells, CD138 (figure 1A). Heparin is a low molecular weight soluble heparan sulfate proteoglycan (HSPG), $NaClO_3$ is an inhibitor of sulfotransferases and heparitinase/chondroitinase ABC are enzymes able to digest HS/CS chains [23],[24],[25],[26]. Use of these reagents except chondroitinase competed with APRIL binding on MOPC-315$_{BM}$ variant cells, showing that only HS chains from CD138 were implicated (figure 1B). We tested two other factors VEGF and HGF, also requiring HSPG binding for activity and implicated in MM development. Western blot analysis in reducing conditions revealed that recombinant HGF contained a homogeneous population of glycosylated molecules resolving at 35 kDa, while recombinant VEGF contained three distinct molecules compatible with non, single and diglycosylated forms (figure 1supA). Recombinant soluble VEGF and HGF bound to the human multiple myeloma cell line L363 in an HSPG dependent manner, since inhibited by heparin (figure 1supB). At variance with APRIL, VEGF and HGF did not bind to MOPC-315$_{BM}$ variant cells (figure 1C). The 10e4 mAb is known to react with native HS chains, while the 3g10 mAb does not, since it reacts only with the stub of the HS chain left after heparitinase digestion [27]. As for APRIL, 10e4 also reacted with a fraction of cells from the MOPC-315$_{BM}$ variant cell line but not from the parental cell line (figure 1D left panel). Heparitinase treatment expectedly abrogated 10e4 reactivity on the MOPC-315$_{BM}$ variant cell line, and all cells from the two cell lines became 3g10 reactive after heparitinase digestion. APRIL binding tightly correlated with 10e4 mAb reactivity (figure 1D right panel). In total, these results indicated that the variant MOPC-315 cell line

contains at least two populations of cells distinguished by their HS chain. One population

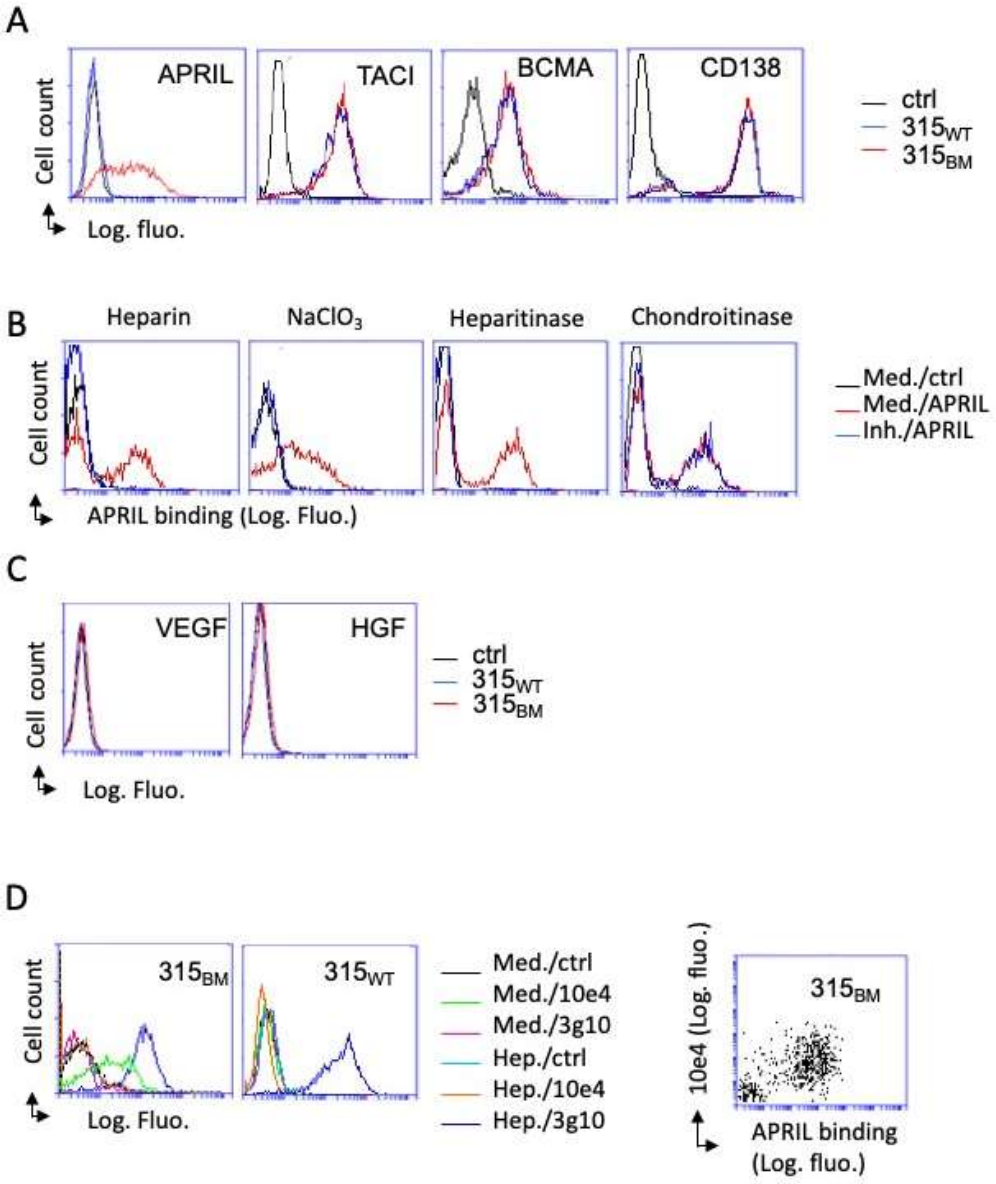

Figure 1: 10e4 reactivity correlates with selective binding of APRIL to MOPC-315BM
Binding of APRIL and expression of the indicated receptors were assessed on MOPC-315BM and MOPC-315WT. Controls (ctrl, muCD40-L for APRIL and isotype-matched Ig for antibodies) were performed on MOPC-315BM cells. B) Binding of soluble APRIL in the presence (Inh.) or absence (Med.) of the indicated inhibitors on MOPC-315BM cells is shown. C) Binding of HGF and VEGF was assessed as in A). D) MOPC-315BM and WT were treated with heparitinase (Hep.) or control medium (Med.). Binding of the anti-HS 10e4 and 3g10 antibodies on the indicated cells is shown (left panel). Ctrl represents isotype-matched control antibodies. Costaining for 10e4 reactivity and APRIL binding on MOPC-315BM cells is also shown (right panel). Plots shown are representative of 3 for A/C, 2 for B/D(left) and 10 for D(right) biological replicates.

expressed a HS chain digestable by heparitinase, reacting with 10e4 and binding APRIL. The other population expressed an HS chain digestable by heparitinase, but neither reacting with 10e4 nor binding APRIL. The latter HS chain is present on all cells from the parental cell line.

10e4 reactivity correlates with ability to develop in the bone marrow

We next sorted the two populations present in the MOPC-315$_{BM}$ variant cell line according to 10e4 reactivity by FACS. Purity exceeded 98% (figure 2A). Cytology analysis of the two populations did not revealed major differences, and confirmed a plasma-cell morphology (figure 2B). *In vitro*, 10e4^{+} cells were less susceptible to all drugs tested including lenalidomide, dexamethasone, melphalan and bortezomib (figure 2C). Ki67 intracellular staining further revealed that all 10e4^{+} cells were proliferative, while about ¼ of the 10e4^{-} cells were quiescent (figure 2D). Upon *in vitro* expansion, we constantly observed cell clumps with 10e4^{+} cells (figure 2E). FSC-H and FSC-A flow cytometry analyses confirmed cell aggregation. These aggregates were more abundant in 10e4^{+} cells with 10,1% +/- 4,1 of the total events compared to 0,4% +/- 0,2 in 10e4^{-} cells (p=0,0001). Expectedly, cell aggregates were also present in the unsorted MOPC-315$_{BM}$ variant cell line. Staining of MOPC-315 cell line for CD138 repeatedly showed a population of viable 7-AAD-excluding CD138$^{low/neg.}$ cells. In figure 2E, These cells represented up to 21% of the cultures. These cells were previously classified as preapoptotic cells in MM cultures [28]. Notably, only 0,1% of the cells present in clumps showed this preapoptotic phenotype, indicating high cell viability. In the MOPC-315$_{BM}$ cell line, 10e4^{+} cells constituted most of the cells clumps (89% +/- 7, n=12). 3-D cultures in methyl cellulose further showed a high ability to form colonies for the 10e4^{+} cells (figure 2F).

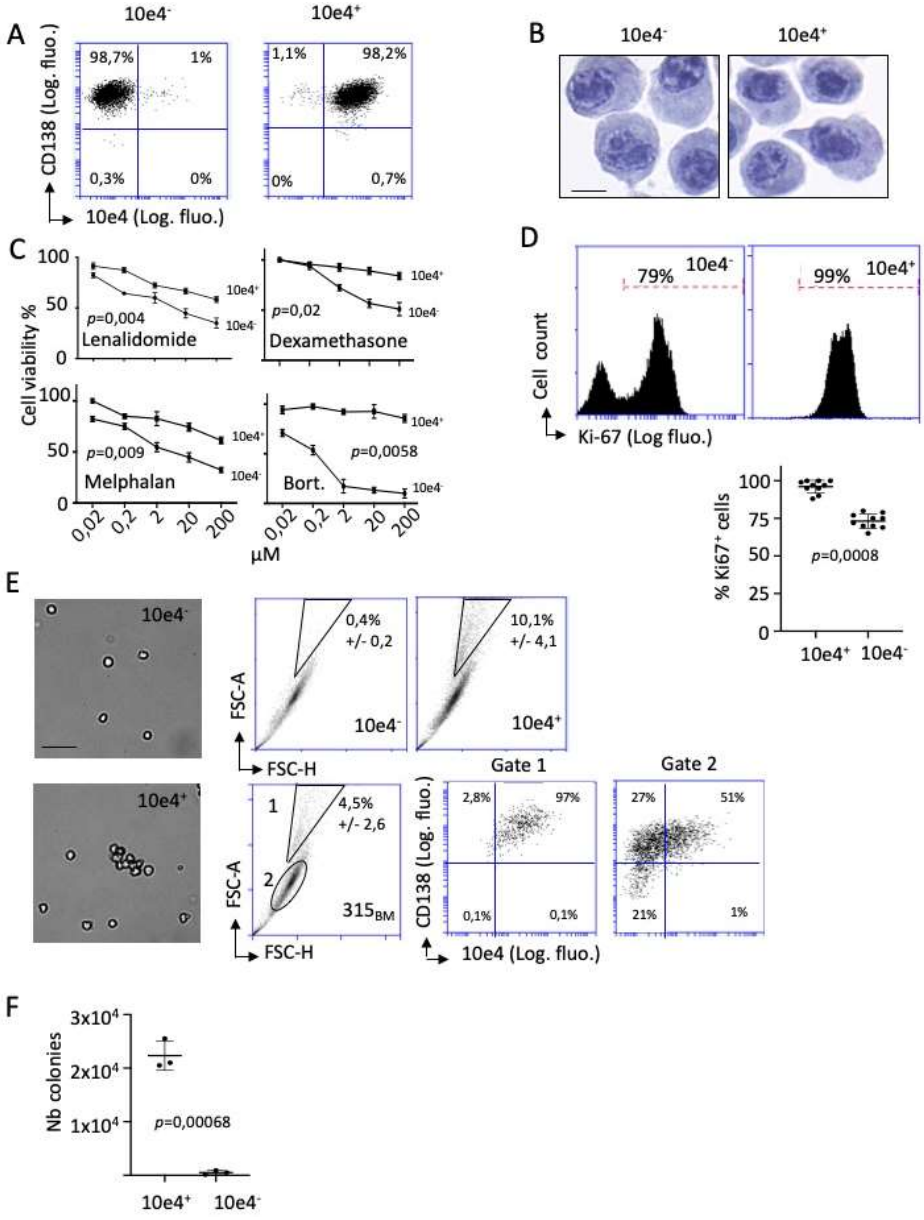

Figure 2: 10e4 positive cells harbors in vitro features of aggressive tumor cells

FACS-sorted 10e4$^+$ and 10e4$^-$ cells were studied *in vitro*. A) Cell purity monitored immediately after FACS sorting is shown. B) Cell cytology was analyzed by Papanicolaou staining. Scale bar: 5 µm. C) *In vitro* drug resistance assay with the indicated concentrations of drugs. D) Intracellular Ki67 staining analyzed by flow cytometry (upper panel) and quantification (bottom panel). E) Picture of an *in vitro* culture (left panel). Scale bar = 50 µm. Cell clumps were analyzed by flow cytometry with the FSC-A/FSC-H parameters (right panel). The MOPC-315$_{BM}$ variant cell line is also shown. F) Quantification of colony formation in methyl cellulose. A/B is representative of two independent FACS sorting experiments. C is representative of 3 biological replicates performed in 3 experimental replicates. D is representative of 9 biological replicates. E is representative of 3 biological replicates except experiments with the MOPC-315$_{BM}$ cell line that was performed in 12 biological replicates. F was performed in 3 experimental replicates.

We next tested tumorigenesis after intravenous injection into syngeneic mice. The latter was performed after a 4-day *in vitro* culture period to allow disappearance of membrane bound 10e4 mAb from the cell surface in order to exclude any *in vivo* antibody-dependent cytoxicity (figure 2sup). BM development of MOPC-315 cells is leading to hind limb paralysis due to spinal cord compression [16]. *In vivo* tumorigenesis was strikingly different, since none of the mice injected with $10e^5$ $10e4^-$ cells showed paralysis, while 100% of the mice did with $10e4^+$ cells by 34 days post injection (figure 3A left panel).

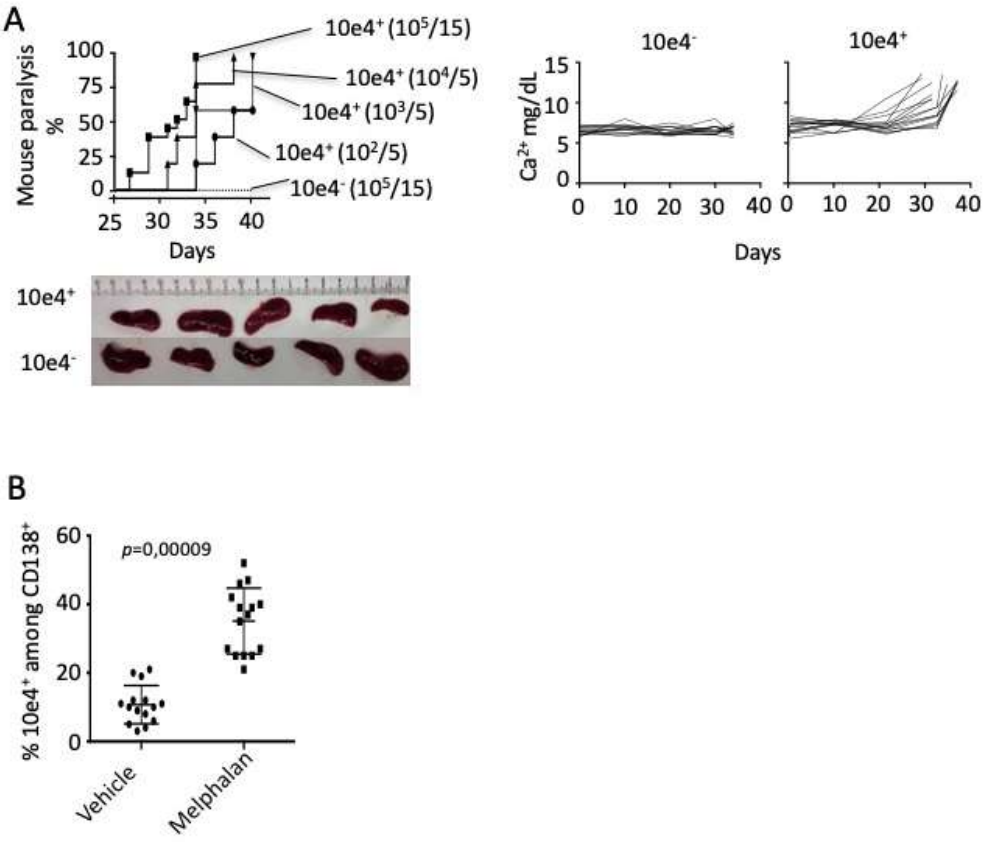

Figure 3: 10e4 positive cells efficiently colonize the bone marrow
FACS-sorted $10e4^+$ and $10e4^-$ cells were studied *in vivo* after intravenous injection. A) Hind-limb paralysis after cell injection into mice (left upper panel). The number of cells/number of mice injected is indicated in brackets. Concentration of Ca^{2+} in serum is shown for mice injected with $10e^5$ cells (right upper panel). Spleen size for mice injected with $10e^5$ cells is shown (bottom panel). B) The MOPC-315$_{BM}$ cell line was injected i.v. and mice were treated with melphalan. BM flushes were analyzed for their content in $CD138^+/10e4^+$ cells. A is representative of 2 independent FACS sortings.

285 Cell titration revealed that as low as $10e^2$ cells from $10e4^+$ cells was enough to induce paralysis,
286 starting at day 34. BM development of MOPC-315 cells is also associated with osteolysis and raise
287 in serum calcium [16]. At euthanasia time for mice injected with $10e4^-$ cells (day 34), serum
288 calcium was in the normal range (6,6 +/- 0,14 mg/dL, n=15). By contrast, serum calcium was
289 significantly higher in mice injected with $10e4^+$ cells (11,38 +/- 0,2 mg/dL, n=15, p<0,0001) at the
290 day of first paralysis signs (figure 3A right panel). Spleen involvement looked similar for the two
291 populations as judged by spleen enlargement and spleen weights (0,68g +/- 0,04 and 0,64g +/-
292 0,02, p=0,38) (figure 3A bottom panel). MOPC-31_{BM} cells were previously shown to be *in vivo*
293 susceptible to melphalan treatment [29]. *In vivo* melphalan treatment revealed that $10e4^+$ cells were
294 more resistant, since their proportion increased after treatment (figure 3B). Taken together, this
295 showed that the $10e4^+$ cells possess high tumorigenesis, colony formation, proliferation, and drug
296 resistance.
297
298 **10e4 positive cells differentiate into 10e4 negative cells**
299 As another approach to separate the two populations, we tried to clone by limiting dilution the
300 MOPC-315_{BM} variant cell line. This invariably gave two different types of clones, one 10e4 fully
301 negative and one with an unexpected mixed population of positive and negative cells indicating
302 variability of 10e4 reactivity among a clonal population (figure 3sup). Analysis of tibia and femur
303 flushes from mice injected with MOPC-315 cells by flow cytometry confirmed the absence of
304 $CD138^+$ MM tumor cells in BM of mice injected with $10e4^-$ cells (figure 4A upper panel). In total,
305 BM flushes from paralyzed mice by development of the positive population contained 5,5% +/- 4
306 $CD138^+$ MOPC-315_{BM} cells among the total cell suspension. The spleen contained $CD138^+$ tumors
307 cells in both cases with 16,2% +/- 4 (n=15) and 18,4 + 3 (n=15) for mice injected with the $10e4^{+and-}$

cells, respectively. Unexpectedly, analysis of gated CD138^{+} cells from BM revealed that more than 2/3 of cells had lost 10e4 reactivity after *in vivo* development (figure 4A bottom panel). Such loss of the 10e4 reactivity was also evidenced in positive cells developing in the spleen. By contrast, the negative population developing in the spleen did not change its 10e4 reactivity, and stayed negative. *In vitro,* we first did not observe major modifications in 10e4 reactivity by expanding the two cell populations as well as the MOPC-315$_{BM}$ variant cell line (figure 4supA). However, growth without medium addition over a 6-day period showed that 10e4^{+} cells gradually lost 10e4 reactivity, starting at day 4 (figure 4B).

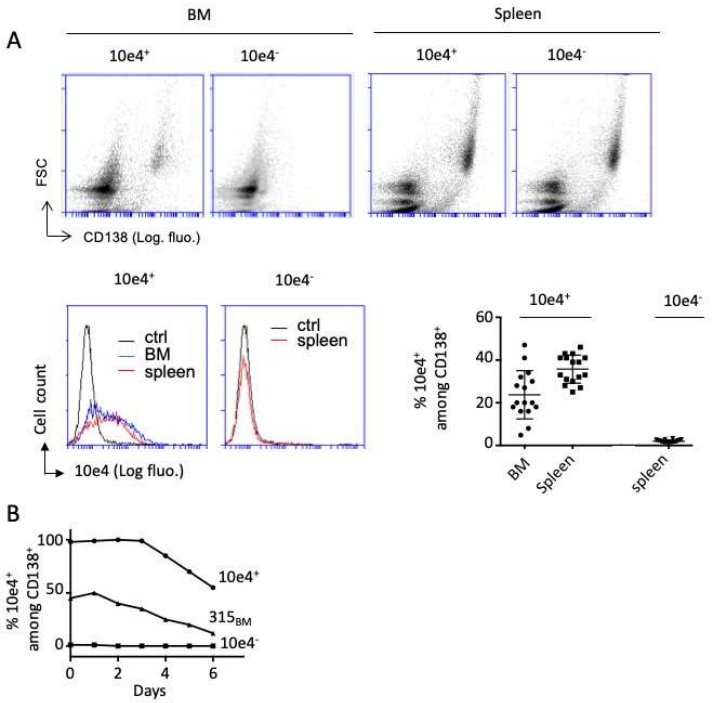

Figure 4: 10e4 reactivity is lost upon cell expansion

A) Cell suspensions of BM flushes and dissociated spleens from tumor-bearing mice were analyzed for the presence of CD138^{+} cells either at paralysis or no later than 34 days after injection of 10e^{5} 10e4^{+} and 10e4^{-} purified cells. Representative dot plots (forward scatter and CD138 fluorescence) are shown (upper panel). The spleen and the bone marrow of tumor-bearing mice were analyzed for the presence of 10e4^{+} MM cells. Relevant histogram plots gated on CD138^{+} MM cells are shown (bottom left panel). Cell quantification is also shown (bottom right panel). B) 10e4 reactivity was followed every day for the two populations expanded *in vitro* in serum-free medium. Data are representative of two independent FACS sorting populations and two biological replicates.

There was again no change for the negative population in this setting. Loss of 10e4 reactivity was also observed with the MOPC-315_{BM} variant cell line. We also used MACS to sort the two populations. The purity obtained ranged at 90% (figure 4supB). An *in vitro* 6-day culture without medium addition of the MACS-sorted positive population confirmed 10e4 reactivity loss (figure 4supC). In this experiment, we also did not detect appearance of $10e4^+$ cells in the negative population. The above data could be explained by a superior proliferative ability for the negative population, outcompeting the positive one. This is unlikely, since we detected a significant decrease in the number of proliferative Ki67 positive cells among the $10e4^-$ population (see figure 3D). Taken together, these showed that $10e4^+$ cells convert into a negative state upon development.

HS3S3Ta1 activity induces 10e4 reactivity, APRIL binding and enables tumorigenesis in BM

We next analyzed expression at the mRNA level of all the enzymes implicated in the synthesis of the heparan core and its sulfation in the parental and variant cell lines. Based on the expression pattern obtained, both populations had the ability to synthesis a heparan chain with a xylose/galactose anchor unit own to the expression of xylosyl (XYLT1, 2) and galactosyl (GALT1, 2) transferases (figure 5A, left panel). The enzymes glucuronyl transferase (GLCAT1) and exotosin(-like) glycosyl transferase (EXT1, 2, L3) adding the disacharride unit of the heparan chain were also detected. The low expression of GLCAT1 in the variant cell line indicates that another enzyme may fulfill this function. Epimerisation of the glucuronic acid into iduronic acid was also possible with the expression of the heparan sulfate glucuronique acid epimerase (HSGLCE). N-sulfation could occur with expression of the N-deacetylase-N-sulfotransferases (NDST1, 2, 3). This pattern of enzyme expression showed that a HS chain was present on CD138 from both cell lines, consistent with the 3g10 reactivity on heparitinase-treated cells previously

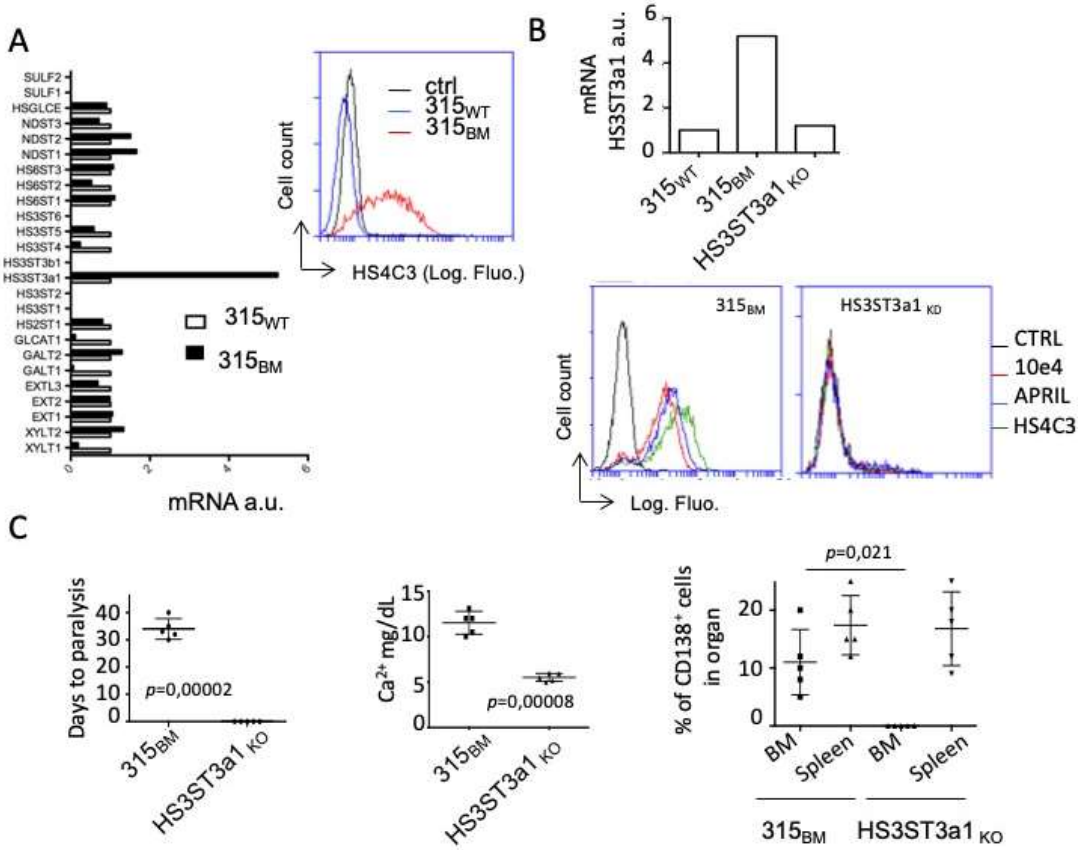

Figure 5: HS3ST3a1 activity promotes BM development

A) qRT-PCR for enzymes involved in HSPG synthesis were quantified in MOPC-315WT and BM cells (left panel). A value of 1 was arbitrarily given to MOPC-315315WT cells. A value of 0 means no detection of the corresponding mRNA. Binding of the anti-HS mAb HS4C3 on the indicated cells is shown (right panel). B) qRT-PCR for HS3ST3a1 mRNA in the indicated cells is shown (upper panel). Binding of the 10e4, HS4C3 mabs and APRIL is shown (bottom panel). C) Mouse paralysis, serum calcium concentration and presence of $CD138^+$ cells in BM and spleen after intravenous injection of the indicated cells are shown with mean +/- SD. Data are representative of 2 for A(left), 3 for A(right)/B, and 2 for C biological replicates.

observed in figure 1D. Final maturation of the HS chain by O-sulfation at position 2, 3 and 6 could also be possible by expression of the respective heparan sulfate sulfotransferases HS2ST, HS3ST and HS6ST. In fact, this analysis revealed that only one of the sulfotransferases adding 3-O sulfates, HS3ST3a1, was upregulated in the variant cell line. HS4C3 is another anti-HS mAb reactive with native forms and detecting 3-O sulfates [30]. Expectedly, the parental cell line was

366 negative, while the variant contained a population of positive cells (Figure 5A right panel). We
367 next generated a HS3ST3a1 deleted variant line (Figure 5B upper panel). This line lost its reactivity
368 to 10e4 and HS4C3 as well as its binding ability to APRIL (Figure 5B bottom panel). Loss in 10e4
369 mAb reactivity is consistent with its known sensitivy to sulfation [31]. Notably, *HS3ST3a1* deleted
370 cells were no more able to develop in mouse BM following intravenous injection as assessed by
371 mouse hind limb paralysis, elevation of serum calcium and detection of $CD138^+$ MM cells in BM
372 flushes by flow cytometry (figure 5C). In total, these showed that HS3ST3a1 activity confers
373 APRIL binding, and drastically modulates MM cell behavior.
374
375 **Variable frequency of $10e4^+$ cells in human MM**
376 Analysis of trephine biopsies from MM patients by serial immunohistochemistry indicated that
377 two populations $CD138^+10e4^+$ and $CD138^+10e4^-$ of MM cells may exist (figure 5sup). Figure 6
378 shows a representative picture obtained from multiplexed immunohistochemistry performed on
379 the same section for one MM patient with a lesion negative for 10e4 reactivity and two others
380 containing a mix population of cells. Analysis of 20 MM patients at diagnosis and before any
381 treatment confirmed that the two populations exist in BM lesions from MM patients. They
382 coexisted at variable frequencies with a mean of 23% +/- 18 among all patients and a range from
383 0% to a maximum of 75% per individual lesion.
384
385
386
387
388

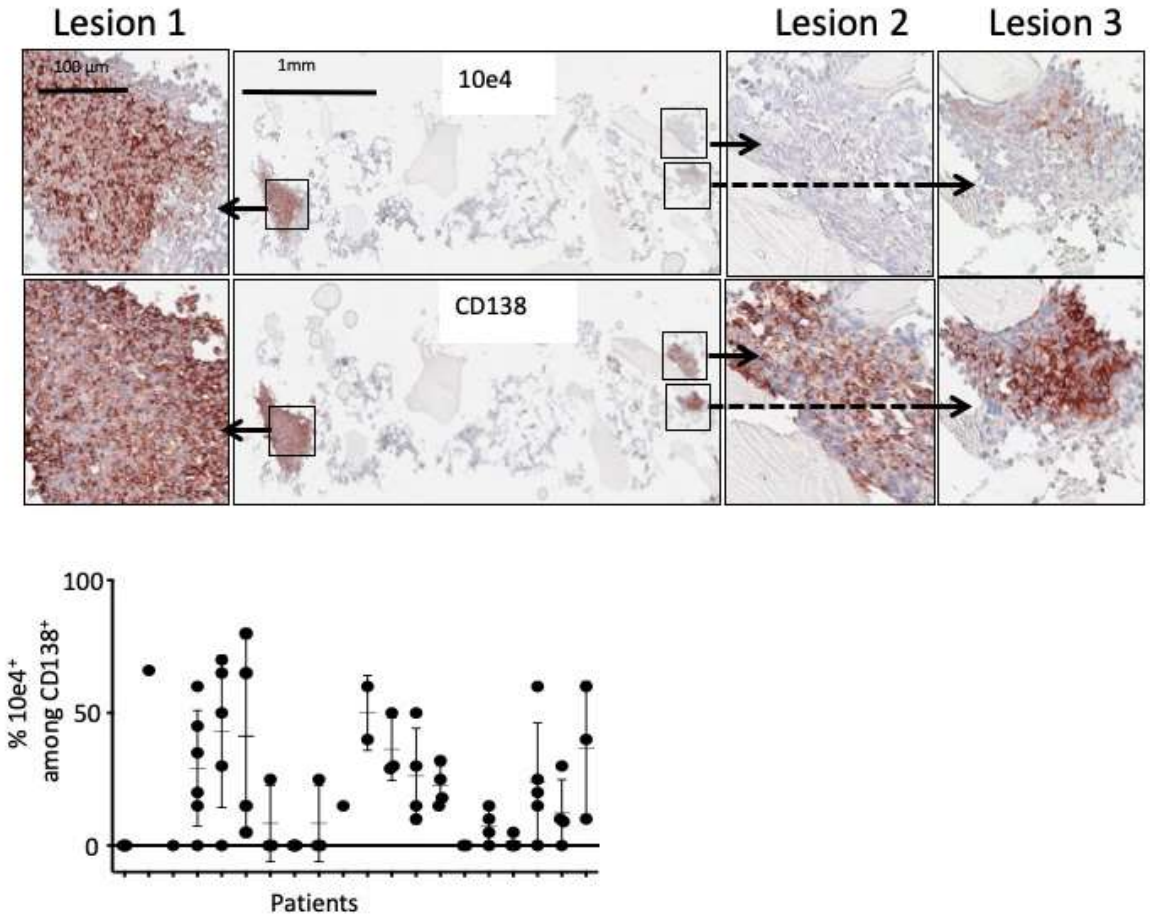

Figure 6: 10e4 positive and negative cells coexist in MM patients BM
A representative picture is shown with magnification on the three MM lesions present in the biopsy (upper panel). Quantification of 10e4$^+$ MM cells from 20 patients was performed at diagnosis. All lesions present on the section were counted. One dot corresponds to one lesion. The mean value +/- SD is indicated.

Discussion

We found that a fine sulfation of the HS chain of CD138 modulates MM behavior. This fine sulfation is achieved by HS3ST3a1, a sulfotransferase that adds a sulfate residue at position 3 on the glucosamine residue. 3-O sulfation on GAG chains is a relatively rare event, despite the fact that 3-O sulfotransferases represent the largest family of all sulfotransferases with 7 members [32]. HS3ST3 is thought to mediate a highly specific 3-O sulfation by adding a sulfate group only on

403 N-unsubstituted glucosamine residues [33],[34]. 3-O sulfation is also the main maturation event
404 involved in determining the ligand specificity [15]. Here, we could confirm the high ligand
405 selectivity, since HS3ST3a1 activity allowed the selective binding to APRIL but not to VEGF-A
406 and HGF.
407 Changes in MM cells resulting from HS3ST3a1 activity are quite drastic. Indeed, HS3ST3a1 active
408 cells possessed high tumorigenesis in BM. *In vitro*, culture of cells with HS3ST3a1 activity
409 revealed the formation of aggregates. The ability of these cells to form colonies was confirmed in
410 a methyl cellulose growth assay. They also have a superior proliferative rate. These cells are also
411 more resistant to drugs both *in vitro* and *in vivo* experimental settings. MOPC-315_{BM} cells have
412 previously been shown to be sensitive to APRIL stimulation [35]. Features observed here for the
413 HS3ST3a1-active population are likely explained, at least in part, by the ability to bind APRIL, if
414 one considers the role described for this factor on MM cell survival, cell cycle progression and
415 drug resistance [4],[36],[37],[38]. Finally, these cells differentiated upon expansion by losing their
416 post-translational modification to acquire a more quiescent state, which could be considered as
417 less aggressive cells. Several features harbored by HS3ST3a1-active cells are shared with cancer
418 stem cells (CSCs). However, we do not believe that these cells represent CSC in MM, since they
419 are definitely too abundant in the BM of MM patients. In addition, CSCs in MM have already been
420 described with a phenotype shifted towards an inactive CD138 with either downregulation of
421 expression or high expression of heparanase [39–41].
422 MM treatment has constantly improved over the last decades with the design of potent MM
423 specific drugs and their combination [42]. Immunotherapy targeting MM surface receptors with
424 the use of either cytotoxic antibodies or their chimeric form transduced into T cells is also
425 contributing. BCMA, one APRIL signaling receptor, is considered as a successful target with the

use of T cells transduced with a chimeric antigen receptor (CAR), and most recent clinical trials targeting BCMA with a bispecific antibody also engaging T cells confirm this statement [43,44]. However, escape variants downregulating BCMA have already been described in MM patients on BCMA-targeting therapies [45],[46]. In some cases, BCMA downregulation may be reversible with a regain susceptibility during a second treatment cycle [47]. However, the identification of BCMA homozygous deletion mutant in MM patients by two independent groups dampens the promise [48],[49]. BCMA is one unique MM receptor triggered by APRIL and to a lesser extent BAFF, since BAFF binding to BCMA is of much lower affinity than APRIL binding to BCMA [50],[51]. Furthermore, *in vitro* functional assays did not reveal a role of trimeric BAFF in the stimulation of BCMA-expressing cells. Occurrence of BCMA full deletion mutant on BCMA-therapies revealed that MM tumors may progress without BCMA stimulation. Drugs targeting several MM receptors at once such as the APRIL- and the related BAFF-CARs may circumvent the emergence of such escape mutants [52],[53],[54]. These drugs will at least target a second signaling receptor on MM cells, TACI. Along this line, CD138 is definitely a valuable target own to its unique ability to bind several MM promoting factors. Targeting the proteic core of CD138 appears unwanted, since CD138 is expressed on other vital cells such as hepatocytes and epithelial cells [55],[56]. A post-translational modification of CD138 as the one described here may be more specific to MM, and could represent a valuable target to continue improving MM treatments.

Authors' contributions: BL, MB, CE, MQ, CO, BPV, ZA, TA, MJ and BH performed experiments. MKT, SN, VKT and BB provided mandatory reagents and/or expertise, MJ, BB and BH analyzed data. BH designed the study and wrote the manuscript.

Funding: Region Auvergne Rhone-Alpes (BH), ligue contre le cancer (BH), and French foundation for the research on monoclonal gammopathies (BH)

References

[1] S.V. Rajkumar, Multiple myeloma: 2022 update on diagnosis, risk stratification, and management, Am J Hematol. 97 (2022) 1086–1107. https://doi.org/10.1002/ajh.26590.

[2] Y. Yang, V. MacLeod, Y. Dai, Y. Khotskaya-Sample, Z. Shriver, G. Venkataraman, R. Sasisekharan, A. Naggi, G. Torri, B. Casu, I. Vlodavsky, L.J. Suva, J. Epstein, S. Yaccoby, J.D. Shaughnessy, B. Barlogie, R.D. Sanderson, The syndecan-1 heparan sulfate proteoglycan is a viable target for myeloma therapy, Blood. 110 (2007) 2041–2048. https://doi.org/10.1182/blood-2007-04-082495.

[3] Z. Ren, M. Spaargaren, S.T. Pals, Syndecan-1 and stromal heparan sulfate proteoglycans: key moderators of plasma cell biology and myeloma pathogenesis, Blood. 137 (2021) 1713–1718. https://doi.org/10.1182/blood.2020008188.

[4] J. Moreaux, A.-C. Sprynski, S.R. Dillon, K. Mahtouk, M. Jourdan, A. Ythier, P. Moine, N. Robert, E. Jourdan, J.F. Rossi, B. Klein, APRIL and TACI interact with syndecan-1 on the surface of multiple myeloma cells to form an essential survival loop, Eur. J. Haematol. 83 (2009) 119–129. https://doi.org/10.1111/j.1600-0609.2009.01262.x.

[5] P.W.B. Derksen, R.M.J. Keehnen, L.M. Evers, M.H.J. van Oers, M. Spaargaren, S.T. Pals, Cell surface proteoglycan syndecan-1 mediates hepatocyte growth factor binding and promotes Met signaling in multiple myeloma, Blood. 99 (2002) 1405–1410.

[6] Z. Ren, H. van Andel, W. de Lau, R.B. Hartholt, M.M. Maurice, H. Clevers, M.J. Kersten, M. Spaargaren, S.T. Pals, Syndecan-1 promotes Wnt/β-catenin signaling in multiple myeloma by presenting Wnts and R-spondins, Blood. 131 (2018) 982–994. https://doi.org/10.1182/blood-2017-07-797050.

[7] A. Purushothaman, T. Uyama, F. Kobayashi, S. Yamada, K. Sugahara, A.C. Rapraeger, R.D. Sanderson, Heparanase-enhanced shedding of syndecan-1 by myeloma cells promotes endothelial invasion and angiogenesis, Blood. 115 (2010) 2449–2457. https://doi.org/10.1182/blood-2009-07-234757.

[8] M.V. Dhodapkar, R.D. Sanderson, Syndecan-1 (CD 138) in myeloma and lymphoid malignancies: a multifunctional regulator of cell behavior within the tumor microenvironment, Leuk. Lymphoma. 34 (1999) 35–43. https://doi.org/10.3109/10428199909083378.

[9] J. Wijdenes, W.C. Vooijs, C. Clément, J. Post, F. Morard, N. Vita, P. Laurent, R.X. Sun, B. Klein, J.M. Dore, A plasmocyte selective monoclonal antibody (B-B4) recognizes syndecan-1, Br. J. Haematol. 94 (1996) 318–323.

[10] K. Mahtouk, F.W. Cremer, T. Rème, M. Jourdan, M. Baudard, J. Moreaux, G. Requirand, G. Fiol, J. De Vos, M. Moos, P. Quittet, H. Goldschmidt, J.-F. Rossi, D. Hose, B. Klein, Heparan sulphate proteoglycans are essential for the myeloma cell growth activity of EGF-family ligands in multiple myeloma, Oncogene. 25 (2006) 7180–7191. https://doi.org/10.1038/sj.onc.1209699.

[11] R.D. Sanderson, Y. Yang, Syndecan-1: a dynamic regulator of the myeloma microenvironment, Clin. Exp. Metastasis. 25 (2008) 149–159. https://doi.org/10.1007/s10585-007-9125-3.
[12] R.M. Reijmers, R.W.J. Groen, H. Rozemuller, A. Kuil, A. de Haan-Kramer, T. Csikós, A.C.M. Martens, M. Spaargaren, S.T. Pals, Targeting EXT1 reveals a crucial role for heparan sulfate in the growth of multiple myeloma, Blood. 115 (2010) 601–604. https://doi.org/10.1182/blood-2009-02-204396.
[13] R. Kokenyesi, M. Bernfield, Core protein structure and sequence determine the site and presence of heparan sulfate and chondroitin sulfate on syndecan-1, J. Biol. Chem. 269 (1994) 12304–12309.
[14] J.K. Langford, M.J. Stanley, D. Cao, R.D. Sanderson, Multiple heparan sulfate chains are required for optimal syndecan-1 function, J Biol Chem. 273 (1998) 29965–29971. https://doi.org/10.1074/jbc.273.45.29965.
[15] L. Kjellén, U. Lindahl, Specificity of glycosaminoglycan-protein interactions, Curr Opin Struct Biol. 50 (2018) 101–108. https://doi.org/10.1016/j.sbi.2017.12.011.
[16] P.O. Hofgaard, H.C. Jodal, K. Bommert, B. Huard, J. Caers, H. Carlsen, R. Schwarzer, N. Schunemann, F. Jundt, M.M. Lindeberg, B. Bogen, A novel mouse model for multiple myeloma (MOPC315.BM) that allows noninvasive spatiotemporal detection of osteolytic disease, PloS One. 7 (2012) e51892. https://doi.org/10.1371/journal.pone.0051892.
[17] F.A. Ran, P.D. Hsu, J. Wright, V. Agarwala, D.A. Scott, F. Zhang, Genome engineering using the CRISPR-Cas9 system, Nat Protoc. 8 (2013) 2281–2308. https://doi.org/10.1038/nprot.2013.143.
[18] T.G. Montague, J.M. Cruz, J.A. Gagnon, G.M. Church, E. Valen, CHOPCHOP: a CRISPR/Cas9 and TALEN web tool for genome editing, Nucleic Acids Res. 42 (2014) W401-407. https://doi.org/10.1093/nar/gku410.
[19] K. Ingold, A. Zumsteg, A. Tardivel, B. Huard, Q.G. Steiner, T.G. Cachero, F. Qiang, L. Gorelik, S.L. Kalled, H. Acha-Orbea, P.D. Rennert, J. Tschopp, P. Schneider, Identification of proteoglycans as the APRIL-specific binding partners, The Journal of Experimental Medicine. 201 (2005) 1375–83. https://doi.org/10.1084/jem.20042309.
[20] J. Hendriks, L. Planelles, J. de Jong-Odding, G. Hardenberg, S.T. Pals, M. Hahne, M. Spaargaren, J.P. Medema, Heparan sulfate proteoglycan binding promotes APRIL-induced tumor cell proliferation, Cell Death and Differentiation. 12 (2005) 637–48. https://doi.org/10.1038/sj.cdd.4401647.
[21] E.J. Bradbury, L.D.F. Moon, R.J. Popat, V.R. King, G.S. Bennett, P.N. Patel, J.W. Fawcett, S.B. McMahon, Chondroitinase ABC promotes functional recovery after spinal cord injury, Nature. 416 (2002) 636–640. https://doi.org/10.1038/416636a.
[22] R. Remark, T. Merghoub, N. Grabe, G. Litjens, D. Damotte, J.D. Wolchok, M. Merad, S. Gnjatic, In-depth tissue profiling using multiplexed immunohistochemical consecutive staining on single slide, Sci Immunol. 1 (2016) aaf6925. https://doi.org/10.1126/sciimmunol.aaf6925.
[23] R. Gupta, M.P. Ponnusamy, Analysis of sulfates on low molecular weight heparin using mass spectrometry: structural characterization of enoxaparin, Expert Rev Proteomics. 15 (2018) 503–513. https://doi.org/10.1080/14789450.2018.1480110.
[24] F. Safaiyan, S.O. Kolset, K. Prydz, E. Gottfridsson, U. Lindahl, M. Salmivirta, Selective effects of sodium chlorate treatment on the sulfation of heparan sulfate, J. Biol. Chem. 274 (1999) 36267–36273. https://doi.org/10.1074/jbc.274.51.36267.

[25] P. Hovingh, A. Linker, The enzymatic degradation of heparin and heparitin sulfate. 3. Purification of a heparitinase and a heparinase from flavobacteria, J. Biol. Chem. 245 (1970) 6170–6175.
[26] E.J. Bradbury, L.D.F. Moon, R.J. Popat, V.R. King, G.S. Bennett, P.N. Patel, J.W. Fawcett, S.B. McMahon, Chondroitinase ABC promotes functional recovery after spinal cord injury, Nature. 416 (2002) 636–640. https://doi.org/10.1038/416636a.
[27] G. David, X.M. Bai, B. Van der Schueren, J.J. Cassiman, H. Van den Berghe, Developmental changes in heparan sulfate expression: in situ detection with mAbs, The Journal of Cell Biology. 119 (1992) 961–75. http://www.ncbi.nlm.nih.gov/pubmed/1385449.
[28] M. Jourdan, M. Ferlin, E. Legouffe, M. Horvathova, J. Liautard, J.F. Rossi, J. Wijdenes, J. Brochier, B. Klein, The myeloma cell antigen syndecan-1 is lost by apoptotic myeloma cells, Br. J. Haematol. 100 (1998) 637–646.
[29] S.S. Riedel, A. Mottok, C. Brede, C.A. Bäuerlein, A.-L. Jordán Garrote, M. Ritz, K. Mattenheimer, A. Rosenwald, H. Einsele, B. Bogen, A. Beilhack, Non-invasive imaging provides spatiotemporal information on disease progression and response to therapy in a murine model of multiple myeloma, PLoS One. 7 (2012) e52398. https://doi.org/10.1371/journal.pone.0052398.
[30] G.B. Ten Dam, S. Kurup, E.M.A. van de Westerlo, E.M.M. Versteeg, U. Lindahl, D. Spillmann, T.H. van Kuppevelt, 3-O-sulfated oligosaccharide structures are recognized by anti-heparan sulfate antibody HS4C3, J Biol Chem. 281 (2006) 4654–4662. https://doi.org/10.1074/jbc.M506357200.
[31] C. Leteux, W. Chai, K. Nagai, C.G. Herbert, A.M. Lawson, T. Feizi, 10E4 antigen of Scrapie lesions contains an unusual nonsulfated heparan motif, J. Biol. Chem. 276 (2001) 12539–12545. https://doi.org/10.1074/jbc.M010291200.
[32] B.E. Thacker, D. Xu, R. Lawrence, J.D. Esko, Heparan sulfate 3-O-sulfation: a rare modification in search of a function, Matrix Biol. 35 (2014) 60–72. https://doi.org/10.1016/j.matbio.2013.12.001.
[33] J. Liu, Z. Shriver, P. Blaiklock, K. Yoshida, R. Sasisekharan, R.D. Rosenberg, Heparan sulfate D-glucosaminyl 3-O-sulfotransferase-3A sulfates N-unsubstituted glucosamine residues, J. Biol. Chem. 274 (1999) 38155–38162. https://doi.org/10.1074/jbc.274.53.38155.
[34] J. Liu, Z. Shriver, R.M. Pope, S.C. Thorp, M.B. Duncan, R.J. Copeland, C.S. Raska, K. Yoshida, R.J. Eisenberg, G. Cohen, R.J. Linhardt, R. Sasisekharan, Characterization of a heparan sulfate octasaccharide that binds to herpes simplex virus type 1 glycoprotein D, J. Biol. Chem. 277 (2002) 33456–33467. https://doi.org/10.1074/jbc.M202034200.
[35] D. Wong, O. Winter, C. Hartig, S. Siebels, M. Szyska, B. Tiburzy, L. Meng, U. Kulkarni, A. Fähnrich, K. Bommert, R. Bargou, C. Berek, V.T. Chu, B. Bogen, F. Jundt, R.A. Manz, Eosinophils and megakaryocytes support the early growth of murine MOPC315 myeloma cells in their bone marrow niches, PLoS One. 9 (2014) e109018. https://doi.org/10.1371/journal.pone.0109018.
[36] Y.-T. Tai, C. Acharya, G. An, M. Moschetta, M.Y. Zhong, X. Feng, M. Cea, A. Cagnetta, K. Wen, H. van Eenennaam, A. van Elsas, L. Qiu, P. Richardson, N. Munshi, K.C. Anderson, APRIL and BCMA promote human multiple myeloma growth and immunosuppression in the bone marrow microenvironment, Blood. 127 (2016) 3225–3236. https://doi.org/10.1182/blood-2016-01-691162.
[37] J. Quinn, J. Glassford, L. Percy, P. Munson, T. Marafioti, M. Rodriguez-Justo, K. Yong, APRIL promotes cell-cycle progression in primary multiple myeloma cells: influence of D-

type cyclin group and translocation status, Blood. 117 (2011) 890–901. https://doi.org/10.1182/blood-2010-01-264424.
[38] J. Moreaux, E. Legouffe, E. Jourdan, P. Quittet, T. Rème, C. Lugagne, P. Moine, J.-F. Rossi, B. Klein, K. Tarte, BAFF and APRIL protect myeloma cells from apoptosis induced by interleukin 6 deprivation and dexamethasone, Blood. 103 (2004) 3148–3157. https://doi.org/10.1182/blood-2003-06-1984.
[39] Y. Kawano, S. Fujiwara, N. Wada, M. Izaki, H. Yuki, Y. Okuno, K. Iyama, H. Yamasaki, A. Sakai, H. Mitsuya, H. Hata, Multiple myeloma cells expressing low levels of CD138 have an immature phenotype and reduced sensitivity to lenalidomide, Int J Oncol. 41 (2012) 876–884. https://doi.org/10.3892/ijo.2012.1545.
[40] Y. Kawano, Y. Kikukawa, S. Fujiwara, N. Wada, Y. Okuno, H. Mitsuya, H. Hata, Hypoxia reduces CD138 expression and induces an immature and stem cell-like transcriptional program in myeloma cells, Int J Oncol. 43 (2013) 1809–1816. https://doi.org/10.3892/ijo.2013.2134.
[41] K. Tripathi, V.C. Ramani, S.K. Bandari, R. Amin, E.E. Brown, J.P. Ritchie, M.D. Stewart, R.D. Sanderson, Heparanase promotes myeloma stemness and in vivo tumorigenesis, Matrix Biol. 88 (2020) 53–68. https://doi.org/10.1016/j.matbio.2019.11.004.
[42] S.K. Kumar, V. Rajkumar, R.A. Kyle, M. van Duin, P. Sonneveld, M.-V. Mateos, F. Gay, K.C. Anderson, Multiple myeloma, Nat Rev Dis Primers. 3 (2017) 17046. https://doi.org/10.1038/nrdp.2017.46.
[43] S.Z. Usmani, A.L. Garfall, N.W.C.J. van de Donk, H. Nahi, J.F. San-Miguel, A. Oriol, L. Rosinol, A. Chari, M. Bhutani, L. Karlin, L. Benboubker, L. Pei, R. Verona, S. Girgis, T. Stephenson, Y. Elsayed, J. Infante, J.D. Goldberg, A. Banerjee, M.-V. Mateos, A. Krishnan, Teclistamab, a B-cell maturation antigen × CD3 bispecific antibody, in patients with relapsed or refractory multiple myeloma (MajesTEC-1): a multicentre, open-label, single-arm, phase 1 study, Lancet. 398 (2021) 665–674. https://doi.org/10.1016/S0140-6736(21)01338-6.
[44] P. Moreau, A.L. Garfall, N.W.C.J. van de Donk, H. Nahi, J.F. San-Miguel, A. Oriol, A.K. Nooka, T. Martin, L. Rosinol, A. Chari, L. Karlin, L. Benboubker, M.-V. Mateos, N. Bahlis, R. Popat, B. Besemer, J. Martínez-López, S. Sidana, M. Delforge, L. Pei, D. Trancucci, R. Verona, S. Girgis, S.X.W. Lin, Y. Olyslager, M. Jaffe, C. Uhlar, T. Stephenson, R. Van Rampelbergh, A. Banerjee, J.D. Goldberg, R. Kobos, A. Krishnan, S.Z. Usmani, Teclistamab in Relapsed or Refractory Multiple Myeloma, N Engl J Med. 387 (2022) 495–505. https://doi.org/10.1056/NEJMoa2203478.
[45] J.N. Brudno, I. Maric, S.D. Hartman, J.J. Rose, M. Wang, N. Lam, M. Stetler-Stevenson, D. Salem, C. Yuan, S. Pavletic, J.A. Kanakry, S.A. Ali, L. Mikkilineni, S.A. Feldman, D.F. Stroncek, B.G. Hansen, J. Lawrence, R. Patel, F. Hakim, R.E. Gress, J.N. Kochenderfer, T Cells Genetically Modified to Express an Anti-B-Cell Maturation Antigen Chimeric Antigen Receptor Cause Remissions of Poor-Prognosis Relapsed Multiple Myeloma, J Clin Oncol. 36 (2018) 2267–2280. https://doi.org/10.1200/JCO.2018.77.8084.
[46] A.D. Cohen, A.L. Garfall, E.A. Stadtmauer, J.J. Melenhorst, S.F. Lacey, E. Lancaster, D.T. Vogl, B.M. Weiss, K. Dengel, A. Nelson, G. Plesa, F. Chen, M.M. Davis, W.-T. Hwang, R.M. Young, J.L. Brogdon, R. Isaacs, I. Pruteanu-Malinici, D.L. Siegel, B.L. Levine, C.H. June, M.C. Milone, B cell maturation antigen-specific CAR T cells are clinically active in multiple myeloma, J Clin Invest. 129 (2019) 2210–2221. https://doi.org/10.1172/JCI126397.

[47] N. Gazeau, D. Beauvais, I. Yakoub-Agha, S. Mitra, T.B. Campbell, T. Facon, S. Manier, Effective anti-BCMA retreatment in multiple myeloma, Blood Adv. 5 (2021) 3016–3020. https://doi.org/10.1182/bloodadvances.2021004176.
[48] M.C. Da Via, O. Dietrich, M. Truger, P. Arampatzi, J. Duell, A. Heidemeier, X. Zhou, S. Danhof, S. Kraus, M. Chatterjee, M. Meggendorfer, S. Twardziok, M.-E. Goebeler, M.S. Topp, M. Hudecek, S. Prommersberger, K. Hege, S. Kaiser, V. Fuhr, N. Weinhold, A. Rosenwald, F. Erhard, C. Haferlach, H. Einsele, K.M. Kortüm, A.-E. Saliba, L. Rasche, Homozygous BCMA gene deletion in response to anti-BCMA CAR T cells in a patient with multiple myeloma, Nat Med. 27 (2021) 616–619. https://doi.org/10.1038/s41591-021-01245-5.
[49] M.K. Samur, M. Fulciniti, A. Aktas Samur, A.H. Bazarbachi, Y.-T. Tai, R. Prabhala, A. Alonso, A.S. Sperling, T. Campbell, F. Petrocca, K. Hege, S. Kaiser, H.A. Loiseau, K.C. Anderson, N.C. Munshi, Biallelic loss of BCMA as a resistance mechanism to CAR T cell therapy in a patient with multiple myeloma, Nat Commun. 12 (2021) 868. https://doi.org/10.1038/s41467-021-21177-5.
[50] E.S. Day, T.G. Cachero, F. Qian, Y. Sun, D. Wen, M. Pelletier, Y.-M. Hsu, A. Whitty, Selectivity of BAFF/BLyS and APRIL for binding to the TNF family receptors BAFFR/BR3 and BCMA, Biochemistry. 44 (2005) 1919–1931. https://doi.org/10.1021/bi048227k.
[51] Y.R. Miao, K. Thakkar, C. Cenik, D. Jiang, K. Mizuno, C. Jia, C.G. Li, H. Zhao, A. Diep, Y. Xu, X.E. Zhang, T.T.C. Yang, M. Liedtke, P. Abidi, W.-S. Leung, A.C. Koong, A.J. Giaccia, Developing high-affinity decoy receptors to treat multiple myeloma and diffuse large B cell lymphoma, J Exp Med. 219 (2022) e20220214. https://doi.org/10.1084/jem.20220214.
[52] L. Lee, B. Draper, N. Chaplin, B. Philip, M. Chin, D. Galas-Filipowicz, S. Onuoha, S. Thomas, V. Baldan, R. Bughda, P. Maciocia, E. Kokalaki, M.P. Neves, D. Patel, M. Rodriguez-Justo, J. Francis, K. Yong, M. Pule, An APRIL-based chimeric antigen receptor for dual targeting of BCMA and TACI in multiple myeloma, Blood. 131 (2018) 746–758. https://doi.org/10.1182/blood-2017-05-781351.
[53] A. Schmidts, M. Ormhøj, B.D. Choi, A.O. Taylor, A.A. Bouffard, I. Scarfò, R.C. Larson, M.J. Frigault, K. Gallagher, A.P. Castano, L.S. Riley, M.L. Cabral, A.C. Boroughs, R.M.-H. Velasco Cárdenas, W. Schamel, J. Zhou, S. Mackay, Y.-T. Tai, K.C. Anderson, M.V. Maus, Rational design of a trimeric APRIL-based CAR-binding domain enables efficient targeting of multiple myeloma, Blood Adv. 3 (2019) 3248–3260. https://doi.org/10.1182/bloodadvances.2019000703.
[54] D.P. Wong, N.K. Roy, K. Zhang, A. Anukanth, A. Asthana, N.J. Shirkey-Son, S. Dunmire, B.J. Jones, W.S. Lahr, B.R. Webber, B.S. Moriarity, P. Caimi, R. Parameswaran, A BAFF ligand-based CAR-T cell targeting three receptors and multiple B cell cancers, Nat Commun. 13 (2022) 217. https://doi.org/10.1038/s41467-021-27853-w.
[55] K.I. Stanford, J.R. Bishop, E.M. Foley, J.C. Gonzales, I.R. Niesman, J.L. Witztum, J.D. Esko, Syndecan-1 is the primary heparan sulfate proteoglycan mediating hepatic clearance of triglyceride-rich lipoproteins in mice, J. Clin. Invest. 119 (2009) 3236–3245. https://doi.org/10.1172/JCI38251.
[56] N. Sturm, M. Quinterot, J.-P. Guyot, C. Righini, W.F. Daamen, T.H. van Kuppevelt, B. Huard, Polarized Secretion of APRIL by the Tonsil Epithelium Upon Toll-Like Receptor Stimulation, Front Immunol. 12 (2021) 715724. https://doi.org/10.3389/fimmu.2021.715724.